Physically Cross-Linked Alkylacrylamide Hydrogels: A SANS Analysis of the Microstructure

Jun Tian,[†,‡] Thomas A. P. Seery,[‡,§] Derek L. Ho,[⊥] and R. A. Weiss*[,†,‡]

Chemical Engineering Department, University of Connecticut, Storrs, Connecticut 06269; Polymer Program, Institute of Materials Science, University of Connecticut, Storrs, Connecticut 06269; Chemistry Department, University of Connecticut, Storrs, Connecticut 06269; and NIST Center for Neutron Research, National Institute of Standards and Technology, Gaithersburg, Maryland 20899

Received March 17, 2004; Revised Manuscript Received October 16, 2004

ABSTRACT: The microstructure of copolymer hydrogels composed of either *N*,*N*-dimethylacrylamide (DMA) or *N*-isopropylacrylamide(NIPA) and 2-(*N*-ethylfluorooctanesulfonamido)ethyl acrylate, FOSA, was studied by small-angle neutron scattering (SANS). The FOSA/NIPA gels exhibited a thermally reversible volume phase transition and a temperature-sensitive microstructure, while the FOSA/DMA gels did not. A modified interacting core−shell microstructure model was used to explain the SANS data for both gels. The cross-link junctions of the gel consisted of nanophase-separated FOSA domains composed of a FOSA core surrounded by a water-poor layer of the alkylacrylamide. The average spherical core radius ranged from 1 to 3 nm, and the average shell thickness ranged from 0 to 1.5 nm; the FOSA aggregation number ranged from 10 to 180. The hydrogels exhibited chain-sized heterogeneities due to solutionlike thermal fluctuations and larger sized heterogeneities due to a solidlike cluster structure. The chain correlation and the large heterogeneities were similar to those observed in covalent DMA and NIPA hydrogels. The chain correlation length ranged from 0.5 to 3.5 nm, and the large heterogeneities ranged from 50 to 90 nm.

A previous paper[1] described the phase behavior and small-angle scattering characterization of the microstructure of hydrophobically modified hydrogels composed of 2-(*N*-ethylperfluorooctanesulfonamido)ethyl acrylate (FOSA) and *N*-isopropylacrylamide (NIPA) or *N*,*N*-dimethylacrylamide (DMA). Aggregation of the FOSA moieties produced a physically cross-linked microstructure. The FOSA/NIPA copolymer hydrogels exhibited a thermally reversible volume phase transition (VPT)[2,3] between a swollen and a collapsed phase, similar to that observed for covalently cross-linked NIPA gels. Increasing the FOSA content decreased the temperature of the VPT (T_{VPT}) and broadened the transition. In contrast, covalently cross-linked DMA hydrogels did not exhibit a VPT, and the introduction of FOSA did not produce a VPT for those copolymers. This paper describes the microstructure of those copolymer gels.

Spatial concentration fluctuations in gels arise from polymer chains in a semidilute polymer solution[4,5] and from static inhomogeneities due to the gel microstructure.[6−9] These can be characterized by using scattering experiments, such as dynamic light scattering (DLS),[10,11] small-angle X-ray scattering (SAXS), and small-angle neutron scattering (SANS),[12−15] and various models of the gel microstructure have been proposed to explain the scattering data. For example, Geissler and coworkers[16,17] proposed a scattering model that combined Gaussian and Lorentzian terms to explain the observation of two characteristic lengths observed by SANS for poly(dimethylsiloxane) (PDMS)/toluene and poly(vinyl acetate) (PVAc)/toluene gels.

The Gaussian term accounts for solidlike contributions to the concentration fluctuations, and the Lorentzian term accounts for liquidlike, local concentration fluctuations. Shibayama et al.[13] used that model to describe the SANS from aqueous NIPA covalent gels and concluded that the VPT of gels may be explained by the three-dimensional Ising model proposed by Li and Tanaka.[18] Recently, Geissler et al.[19,20] used another expression that combined a Lorentzian function[4,5] that described short-range concentration fluctuations and a Debye−Bueche[21] term that accounted for longer range static fluctuations from covalently connected cross-links to describe the SANS from PDMS/hexane, PDMS/octane, PDMS/toluene, and PVAc/toluene gels. Horkay et al.[22] observed a third inhomogeneity in the SANS of poly(isoprene)/toluene gels due to "dense clusters" and used a second Debye−Bueche type term to account for the excess scattering from the clusters.

The objective of this paper was to characterize the effects of hydrophobic interactions and temperature on the microstructure of FOAS/NIPA and FOSA/DMA gels. The study employed small-angle neutron scattering (SANS), and the behavior of the physical gels was compared with that of chemically cross-linked NIPA and DMA hydrogels.

Experimental Section

Materials. *N*,*N*-Dimethylacrylamide (DMA, 99%), *N*-isopropylacrylamide (NIPA, 99%), and 2-(*N*-ethylperfluorooctanesulfonamido)ethyl acrylate (FOSA) were obtained from Aldrich Chemical Co., Acros Chemical Co., and 3M Co., respectively. The structures of these monomers are shown in Scheme 1. The synthesis of the FOSA/DMA and FOSA/NIPA copolymers was described in a previous paper.[1] The copolymers that were synthesized and used in this study are summarized in Table 1. The nomenclature used in this paper for the DMA/FOSA and NIPA/FOSA copolymers is DF*xx* and NF*xx*, respectively, where *xx* represents the mol % FOSA. Except where noted, the T_{VPT} was determined by swelling measurements.[1]

The preparation of chemical cross-linked NIPA and DMA gels was described in a previous paper.[1] *N*,*N*′-Methylenebis-

[†] Chemical Engineering Department, UConn.
[‡] Institute of Materials Science, UConn.
[§] Chemistry Department, UConn.
[⊥] National Institute of Standards and Technology.
* Corresponding author: e-mail rweiss@mail.ims.uconn.edu.

10.1021/ma049474z CCC: $27.50
Published on Web 12/03/2004

Scheme 1. Structure of the Monomers Used

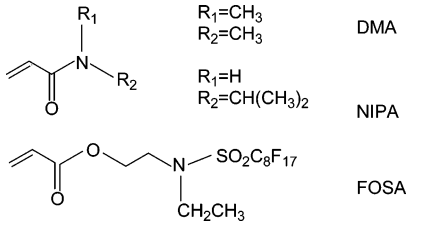

Table 1. Characterization Results of Polymers

polymer ID	FOSA mol %	FOSA wt %	DMA or NIPA (mol %)	T_g (°C)	M_w (10^4 Da)	M_n (10^4 Da)	T_{VPT}[a] (°C)
polyFOSA			0	44.5			
polyDMA			100	124.0	8.6	3.8	
DF5	4.9	25	95.1	110.7	7.3	3.8	
DF9	9.0	38	91.0	99.6	5.6	2.9	
DF17	16.5	56	83.5	94.8	7.7	3.4	
DF22	21.5	63	78.5	88.8	7.6	5.1	
polyNIPA			100	145.1	7.2	4.8	32.3
NF2	2.0	10	98	138.4	5.6	3.4	28
NF5	5.4	24	94.5	130.6	6.4	3.4	17.8
NF8	7.7	32	92.3	128.2	7.2	4.2	15.1
NF10	10.2	39	89.8	126.0	7.1	4.3	13.1

[a] T_{VPT} for polyNIPA was determined by DSC.

(acrylamide), BIS (Aldrich, 98%), was used as the cross-linker, *N,N,N′,N′*-tetramethylethylenediamine, TEMED (Aldrich, 99%), was used as the initiator, ammonium persulfate (Acros, CAS grade) was used as the accelerator, and deuterium oxide, D_2O (Fisher, 99.8% atom d), was used as the solvent. The gel was washed with excess D_2O and then cut into ~2 mm thick disks for SANS measurements. The DMA and NIPA gel characteristics are listed in Table 2.

Copolymer films for neutron scattering measurements were prepared by casting in acetone or THF solution onto glass. The cast film was dried at room temperature for 24 h and then overnight at 60 °C. The dry film was then immersed into deionized water or D_2O/H_2O water mixtures to swell the gel and remove it from the glass. Disks, 18 mm diameter, were cut from the swollen gels for SANS measurements.

SANS. Small-angle neutron scattering (SANS) measurements were performed at the NIST Center for Neutron Research (Gaithersburg, MD). Most data were collected on the NG3 SANS 30 m facility using a q range of 0.035−4.4 nm^{-1} (d = 1.4−179 nm). A cold neutron source with an average wavelength of $\lambda = 0.60$ nm with $\Delta\lambda/\lambda = 14\%$ was used. Contrast variation experiments were performed on the NG1 SANS 8 m facility using an average wavelength of $\lambda = 0.50$ nm with $\Delta\lambda/\lambda = 12\%$ and a q range of 0.10−2.0 nm^{-1} (d = 3.1−63 nm). The sample chamber was a titanium cell with two quartz windows sealed with rubber O-rings, and it was attached to a multiple position sample stage with a temperature controlling circulator. The cell was filled with water to maintain equilibrium hydration of the gel during the experiment. The time-averaged scattering intensity was recorded with a two-dimensional detector.[23] Data were corrected for detector inhomogeneity, transmission, background, and empty cell scattering, and the scattering was calibrated for absolute intensity using a standard reference silica sample from NIST. The 2-dimensional data were circularly averaged to calculate $I(q)$, which was corrected for incoherent scattering from hydrogen by subtracting the plateau value at high q.[24]

Results and Discussion

SANS: Compositional Effects. In a previous paper,[1] nanophase separation of FOSA-rich domains was determined using small-angle X-ray scattering (SAXS). A distinct advantage of neutron scattering over X-ray scattering is that the contrast between different phases can be conveniently tuned to selectively investigate the internal structure of materials. This method exploits the large difference in the neutron scattering length density (SLD) of hydrogen and deuterium. Accordingly, the SLD contrast between different phases in a hydrogel can be adjusted by using mixtures of D_2O and H_2O as the solvent.

The SLDs of NIPA, DMA, FOSA, and various D_2O/H_2O mixtures are given in Table 3. If one assumes that the water resides only in the hydrophilic alkylacrylamide phase, at equilibrium hydration of the copolymers, i.e., >100% water per dry polymer, the SLD of the hydrophilic phase is relatively insensitive to water concentration, and SANS contrast matching of the water-swollen alkylacrylamide and water-depleted FOSA phases occurs at an isotopic ratio of D_2O/H_2O (v/v) ~ 50/50. The contrast matching between the water and DMA or NIPA species occurs for D_2O/H_2O ~ 20/80.

Figure 1 compares the SANS of the NF5 and DF9 physical gels with those of NIPA and DMA covalently cross-linked gels. The combined Gaussian and Lorentzian model that was previously used by Shibayama et al.[13] to fit SANS for NIPA gels did not produce a satisfactory fit of the data in Figure 1 for the covalent NIPA and DMA gels. That may be a consequence of the lower values of q measured in the present study, which resolved additional large heterogeneities not observed by Shibayama et al. Horkay et al.[22] used a three-term model for polyisoprene/toluene gels, eq 1, to account for various size inhomogeneities.

$$I_{gel}(q) = \frac{A_1}{1 + q^2\xi^2} + \frac{A_2}{(1 + q^2\Xi_1^2)^2} + \frac{A_3}{(1 + q^2\Xi_2^2)^2} \quad (1)$$

The first term on the right side of the equation is a Lorentzian function that accounts for the short-range, thermal fluctuations of the chain in a semidilute solution[4,5] (ξ is often called the blob size[4]), and the second and the third terms are longer range, static contributions[21] arising from the elastic constraint Ξ_1 due to the cross-linking and a larger heterogeneity Ξ_2, due to a solidlike structure. A_1, A_2, and A_3 are constants. That model successfully fit the NIPA and DMA gel data (see the solid curves in Figure 1), and the parameters obtained from eq 1 are summarized in Table 2. Although the volume fraction of the network for both gels was almost identical, ~0.07, the NIPA gel exhibited a larger chain correlation length, ξ, larger cross-linking inhomogeneity, Ξ_1, but smaller solidlike inhomogeneity, Ξ_2, than the DMA gel. Those differences indicated that the microstructure of NIPA gels was less homogeneous at smaller length scales but more homogeneous at larger length scales than the DMA gel.

Table 2. Gel Specification and Fitted Structure Parameters[a]

gel ID	monomer concn, mM	cross-linker concn, mM	vol fraction of network ϕ	chain correlation ξ, nm	cross-linking inhomogeneity Ξ_1, nm	large inhomogeneity Ξ_2, nm
DMA	503.1	22.3	0.068	1.5(0.2)	3.8(0.2)	81.8(11)
NIPA	689.2	23.7	0.065	2.6(0.2)	6.8(0.3)	34.9(2.4)

[a] The value in parentheses is the standard deviation from the fit. The gel specification is for the gel at preparation, and the fitted parameters are from SANS at 12.6 °C.

Table 3. Scattering Length Densities of Monomers and Various D_2O/H_2O Mixtures

material		SLD (10^{-6}/nm^2)
NIPA		0.811
DMA		0.896
FOSA		2.830
H_2O	D_2O	
100	0	−0.560
91.9	8.1	0
80	20	0.807
50	50	2.870
30	70	4.250
0	100	6.330

The model given by eq 1, however, did not adequately fit the SANS data for the physical gels shown in Figure 1. For those gels, a core−shell model composed of polydisperse spherical FOSA nanodomains surrounded by a water-poor shell of the alkylacrylamide (see Figure 2) was used to describe the microstructure. The water-poor shell of the alkylacrylamide is presumably comprised of the chain segments that are attached to the FOSA repeat units and which have restrictions on their mobility due to the covalent attachment to the FOSA nanodomains. The core−shell particles are nonuniformly dispersed in the water-swollen alkylacrylamide matrix due to heterogeneities in the spatial arrangement of the physical cross-links.

The model used to fit the SANS data followed that developed for copolymer micelles by Pederson,[25] who used a monodisperse distribution of spherical particles in which a core−shell form factor was combined with a

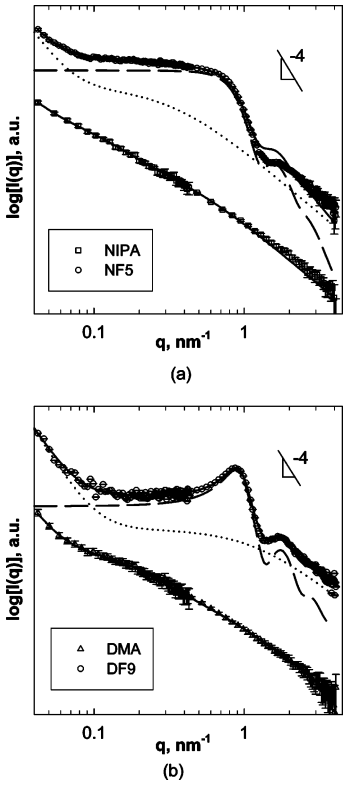

Figure 1. SANS for (a) NF5 and NIPA gels and (b) DF9, DMA gels swollen with pure D_2O at 12.6 °C. The data for NF5 and DF9 gels obtained for different q ranges (see Experimental Section) were rescaled for clarity. The solid curves are the model fits (see text), the dashed ones represent the contribution from the modified core−shell model (eq 2), and the dotted curves are the contribution from chain correlation and large inhomogeneities. The water contents are 180 and 287 wt % for the DF9 and NF5 gels, respectively.

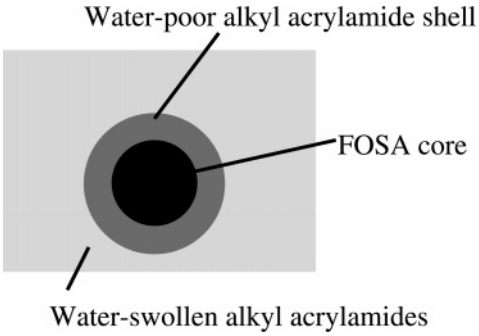

Figure 2. Schematic of core−shell structure of water-swollen DF and NF gels.

hard-sphere model for the structure factor. It was modified here to include a polydisperse distribution; the coherent scattering intensity is given by eq 2.

$$I(q) = cF^2(q)\,S(q) \tag{2}$$

where $F^2(q)$ is the form factor for intraparticle interference and $S(q)$ is the effective structure factor accounting for the interparticle interference of spherical domains and c is a constant. The polydispersity of the particles was accounted for by using the expression for polydisperse core−shell particles proposed by Bartlett and Ottewill[26]

$$\overline{F^2}(q\bar{r}_c) = \int_0^\infty G(r_c)\,F^2(qr_c)\,\mathrm{d}r_c \tag{3}$$

where r_c is the radius of the core, $\bar{r}_c$ is the average core radius, and $G(r_c)$ is the probability density function of the particle radius. An equation for polydisperse interacting hard spheres derived by Griffith et al.[27] using Percus−Yevick closure[28] was used for the effective structure factor

$$S(q) = 1 + \frac{\int_0^\infty\int_0^\infty P_i(q)\,P_j(q)\,H_{ij}(q)\,G(\sigma_i)\,G(\sigma_j)\,\mathrm{d}\sigma_i\,\mathrm{d}\sigma_j}{\int_0^\infty P_i^{\,2}(q)\,G(\sigma_i)\,\mathrm{d}\sigma_i} \tag{4}$$

where P is the scattering amplitude, σ is the particle diameter, $G(\sigma)$ is the particle size distribution function, and $H_{ij}(q)$ is the pair correlation function, with the subscripts referring to the two particles i and j. A Schulz distribution was used because of its mathematical simplicity.

The complete model used for the physical hydrogels, eq 5, was a linear combination of the model for polydisperse spheres, eq 2, and that used by Horkay et al.[29] for covalent gels, eq 1, except that the second term of the Horkay et al. expression was eliminated. That term describes the scattering contribution from the cross-linking inhomogeneities, which is already accounted for by eq 2.

$$I(q) = cF^2(q)\,S(q) + \frac{A_1}{1 + q^2\xi^2} + \frac{A_3}{(1 + q^2\Xi_2^{\,2})^2} \tag{5}$$

This model provides values for the radius of the nanodomain core, r_c, the thickness of the shell, t, the size polydispersity, p, the effective hard-sphere radius, r_{eff}, the effective volume fraction of hard spheres, ϕ_{eff}, and two correlation lengths for the gel inhomogeneities, ξ and Ξ_2. The effective size and volume fraction of the

Table 4. Fitted Structure Parameters of DF and NF Gels[a]

gel ID	T, °C	p	r_c, nm	t, nm	r_{eff}, nm	ϕ_{eff}	ξ, nm	Ξ_2, nm	r_0, nm	ϕ_0	N_{agg}
DF5[b]	9	0.12	1.8(0.006)	1.2(0.1)	3(0.02)	0.19(0.02)	1.0(0.4)	12.8(1.4)	1.8	0.04	34
DF9	12.6	0.15	2.4(0.07)	0.6(0.1)	3.3(0.1)	0.41(0.01)	0.8(0.2)	89.9(20.6)	2.2	0.12	67
	24.8	0.15	2.4(0.07)	0.7(0.08)	3.3(0.09)	0.4(0.008)	1.2(0.2)	82.4(18.1)	2.2	0.12	68
	28.8	0.15	2.4(0.06)	0.7(0.08)	3.3(0.005)	0.39(0.006)	1.5(0.1)	85.6(12.3)	2.2	0.12	70
	33.5	0.15	2.4(0.1)	0.8(0.1)	3.2(0.02)	0.36(0.01)	1.8(0.2)	86.5(21.4)	2.3	0.13	75
	42.5	0.15	2.3(0.05)	0.9(0.06)	3.1(0.007)	0.34(0.006)	2.4(0.09)	93.8(16.6)	2.3	0.13	72
DF17[b]	9	0.11	1.9(0.005)	1.2(0.04)	3.3(0.004)	0.35(0.005)	1.6(0.2)	53.9(10.7)	2.8	0.21	137
DF22	12.6	0.1	1.8(0.2)	1.0(0.2)	3.2(0.02)	0.41(0.02)	0.8(0.09)	76.5(18.8)	2.9	0.31	157
	24.8	0.1	1.9(0.1)	1.1(0.2)	3.1(0.07)	0.4(0.03)	0.4(0.3)	81.0(19.8)	2.9	0.31	147
	28.8	0.1	2.1(0.07)	0.8(0.2)	3.1(0.01)	0.39(0.02)	0.6(0.2)	92.4(22.8)	2.9	0.32	155
	33.5	0.1	2.2(0.08)	0.9(0.2)	3.2(0.03)	0.41(0.02)	1.1(0.2)	89.7(21.7)	3.0	0.32	162
	42.5	0.1	2.4(0.1)	0.8(0.2)	3.2(0.02)	0.4(0.03)	1.1(0.1)	91.6(22.1)	3.0	0.34	177
NF2[b]	9	0.24			2.6(0.2)	0.1(0.01)		12.1(6.9)	1.0	0.01	6
	12.6	0.23			2.6(0.03)	0.07(0.01)		10.3(2.0)	1.0	0.01	7
	16.4	0.25			2.6(0.03)	0.07(0.01)		6.0(0.4)	1.0	0.01	6
	20.4	0.21			2.7(0.05)	0.05(0.02)		5.9(0.2)	1.1	0.01	9
NF5	12.6	0.23	1.9(0.2)	1.3(0.3)	2.7(0.01)	0.19(0.03)	3.0(0.3)	55.0(11.0)	1.7	0.05	29
NF5[b]	9	0.19	1.8(0.01)	0.9(0.1)	3.4(0.08)	0.30(0.02)	0.35(0.33)	3.2(0.09)	1.8	0.05	35
	12.6	0.2	1.8(0.09)	1.0(0.04)	3.3(0.1)	0.23(0.01)	0.42(0.41)	3.8(0.07)	1.9	0.05	46
	16.4	0.23	1.8(0.02)	0.9(0.06)	2.6(0.1)	0.11(0.02)	1.2(0.8)	4.8(0.2)	2.0	0.05	52
NF8[b]	9	0.25	1.8(0.03)	1.5(0.1)	2.8(0.03)	0.39(0.01)	1.6(0.2)	4.6(0.2)	1.8	0.1	35
	12.6	0.31	1.6(0.02)	0.8(0.08)	2.6(0.2)	0.21(0.02)	3.4(0.9)	6.1(0.6)	2.1	0.11	59
NF10	12.6	0.24	1.8(0.2)	1.3(0.6)	2.2(0.02)	0.25(0.2)	1.2[c]	119[c]	2.0	0.15	49

[a] The value in parentheses is the standard deviation. All the standard deviations for $\boldsymbol{p}$ are less than 0.01. [b] Fit was done on SANS data for gels swollen in a (10/90) D_2O/H_2O mixture. [c] The value is not statistically significant.

spherical particles obtained from the fit of eq 5 to the SANS data were larger than those calculated from swelling measurements. That result is similar to what is seen in systems where a repulsive potential between particles produces a larger effective particle size;[30,31] i.e., the distance of closest approach of the particles is larger than the particle diameter.

For both copolymer gels, the fit of eq 5 to the SANS data was reasonably good (Figure 1). The fitted structural parameters are summarized in Table 4. The upturn at low q is due to the scattering from large concentration fluctuations in the gels arising from the clustering of the polymer due to the nonuniform swelling. The large inhomogeneities, Ξ_2 of 55.0 nm for NF5 gels and 89.9 nm for DF9 gels, are similar to those seen in chemical gels, e.g., 34.9 nm for NIPA gels and 81.8 nm for DMA gels (see Tables 2 and 4). In addition, the chain correlation length, ξ, was 0.8 nm for the DF9 gels and 3.0 nm for the NF5 gels, which are also similar to the values in the DMA and NIPA gels. The contributions from both length scale inhomogeneities are represented by the dotted curves in Figure 1, which are similar to the scattering curves for the chemical NIPA and DMA gels. However, the core−shell nanodomains that constitute the cross-link junctions in the physical gels produce the additional scattering illustrated by the dashed curves in Figure 1. The nanodomain size, i.e., the sum of the core radius and the shell thickness, $r_c + t$, for the NF5 and the DF9 gels was 3.2 and 3.0 nm, respectively. The scattering peak at $q_{max} \sim 0.8$ nm^{-1} corresponds to an *inter*particle correlation length, and the peak at $q_{max} = 1.7$ nm^{-1} arises from an *intra*particle correlation (i.e., from the form factor). The mean radius of the core−shell particles was also estimated from the peak in the form factor to be 3.4 nm using the relation[32]

$$r_a = k/q_{max} \tag{6}$$

where q_{max} is the peak position for the maximum in the form factor for spherical particles and $k = 5.76$ is the characteristic value for the first maximum in the form factor for $q > 0$.[32] The two methods of calculating the nanodomain size showed reasonable agreement.

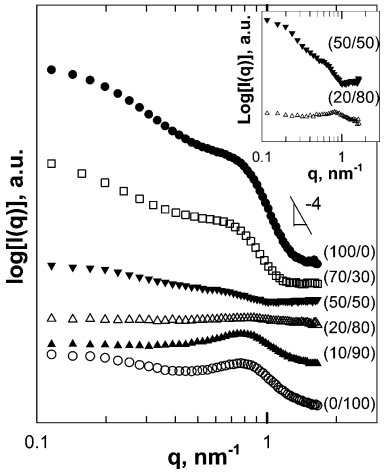

Figure 3. SANS for water-swollen NF5 gels at 10 °C using different ratios of D_2O/H_2O (the numbers in parentheses correspond to the D_2O/H_2O ratio (v/v) in the water mixture) as the solvent. The curves were rescaled to improve clarity for comparisons. The water content was ~300 wt %.

Figure 3 shows the effect of contrast variation using different ratios of D_2O/H_2O on the SANS for the NF5 gels at 10 °C, which is below the VPT for NF5. Those data were not corrected for incoherent scattering because of the narrow q range that was used. The differences in the SANS patterns are due to changes in the relative contribution to the total scattering from either the core−shell or the water-swollen acrylamide matrix as the water contrast changed. For pure H_2O, a scattering peak is observed at $q_{max} = 0.75$ nm^{-1} ($d = 8.4$ nm), which corresponds to the interdomain spacing. When the D_2O/H_2O ratio was 20/80, the peak at $q_{max} = 0.75$ nm^{-1} ($d = 8.4$ nm) became very weak due to the lower contrast between the FOSA nanodomains and the matrix; this is most clearly seen in the inset in Figure 3. At that D_2O/H_2O ratio, the water and the alkylacrylamide chains were contrast matched; therefore, the inhomogeneities in the water-swollen alkylacrylamide phase were not resolved.

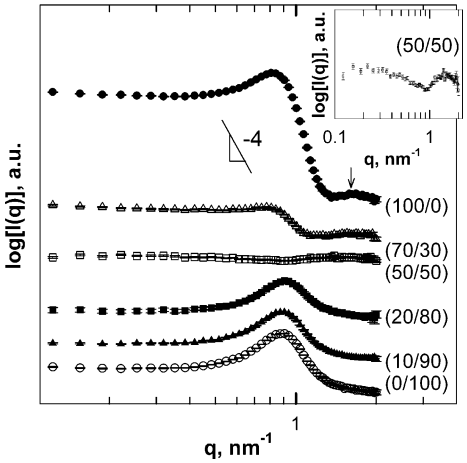

Figure 4. SANS for water-swollen DF9 gels at 12 °C using different ratios of D_2O/H_2O (the numbers in parentheses correspond to the D_2O/H_2O ratio (v/v) in the water mixture) as the solvent. The curves were rescaled to improve clarity for comparisons. The water content was ~180 wt %.

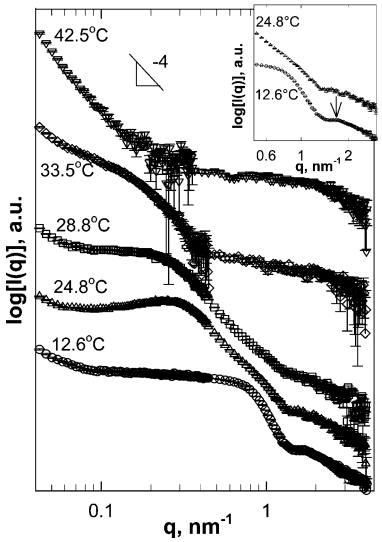

Figure 5. Temperature-dependent SANS for NF5 gels swollen with D_2O. The curves obtained for different q ranges (see Experimental Section) were rescaled to improve clarity for comparisons. The SANS data for the NF5 gel at 12.6 °C are the same shown in Figure 1a. The water contents for the samples at 12.6, 24.8, 28.8, 33.5, and 42.5 °C were about 287, 120, 110, 105, and 105%, respectively.

When the D_2O/H_2O ratio was increased to 50/50, another contrast matching condition was obtained between the FOSA core of the nanoparticles and the water-swollen acrylamide matrix (see Table 3). In that case, the scattering from the FOSA particles is lost and scattering is seen only between the hollow spherical shell of the nanoparticles and the gel matrix and within the gel, i.e., between the chains and the water.

When the D_2O/H_2O ratio was >50/50, the peak due to the inter-nanodomain correlation reappeared at about $q = 0.75$ nm^{-1}, but the peak was distorted due to the SLD profile. When pure D_2O was used as the solvent, Porod behavior, where the intensity decreased as q^{-4}, was observed for $q = 0.8-1.2$ nm^{-1} (see Figure 3), which indicated a sharp interface between the FOSA nanodomains and the hydrophilic matrix. A low-q scattering upturn as seen in Figure 1a is not observed in Figure 3 because of the limited q range used.

The effect of changing the D_2O/H_2O ratio on the SANS of DF9 gels at 12 °C is shown in Figure 4. A scattering peak due to an *inter*domain correlation occurrs at $q_{max} = 0.9$ nm^{-1} ($d = 7.0$ nm) for the swollen gel. As with the NF5 gel, increasing the D_2O/H_2O ratio from 0/100 to 50/50 decreased the intensity of the scattering peak due to a reduction of the contrast between the water-swollen alkylacrylamide phase and the FOSA nanodomains. The scattering peak at $q = 0.9$ nm^{-1} disappeared when the D_2O/H_2O ratio was 50/50, which, like the scattering shown in Figure 3 for the NF5 gels, is consistent with the prediction shown in Table 3 for contrast matching the gel phase and the FOSA nanodomains. However, unlike the scattering results for the NF5 gel at this contrast matching condition, the DF9 gel shows no upturn in the scattering intensity at low q (see the inset in Figure 4). For $D_2O/H_2O = 50/50$, the SANS should be dominated by the empty spherical shell of the nanodomains and the inhomogeneities within the water-rich phase, i.e., between the DMA chains and the water. The absence of an upturn in the DF9 data indicates that the gel phase of the hydrated DF9 was much more homogeneous than for the hydrated NF5 sample.

As with the SANS for the NF5 gels, when the D_2O/H_2O > 50/50, Porod behavior was observed (see Figure 4), which indicates a sharp interface between the nanodomains and the acrylamide/water phase. In addition, Figure 4 shows that the scattering peak due to *inter*domain interference of the FOSA nanodomains reappeared at $q_{max} = 0.82$ nm^{-1} ($d = 7.7$ nm), and a second scattering peak due to the form factor (i.e., an *intra*domain correlation) became more evident at $q_{max} = 1.7$ nm^{-1} (see arrow).

The variation of the scattering patterns with the different D_2O/H_2O ratios supports the contention that the gels do not have a simple two-phase structure. The core−shell model proposed herein appears to be consistent with the scattering, though it should be noted that the model possesses a large number of adjustable parameters. Still, as will be discussed below, many of the parameters were insensitive to changes in the gel composition, which lends some credence to their validity, and the values of the structural parameters seem to be realistic.

SANS: Temperature Effects. The swelling and thermal analysis data presented in a previous paper[1] showed that the NF gels exhibited a temperature-induced VPT, but the DF gels did not. The temperature dependence of the microstructure of those gels was evaluated using SANS of samples swollen with either D_2O or a (10/90) D_2O/H_2O mixture.

Figure 5 shows the SANS for the NF5/D_2O gel for a temperature range of 12−43 °C, which brackets the VPT for that gel. As discussed previously, for 12.6 °C, the scattering peak at $q_{max} = 1.7$ nm^{-1} (see arrow in inset) is due to the form factor for the spherical core−shell nanodomains and corresponds to a radius of $r_0 = 3.4$ nm. This nanodomain size is the same as that seen for the DF9 gels shown in Figure 4. $T_{VPT} = 17.8$ °C for the NF5 gel (see Table 1), and when the temperature was increased to 24.8 °C, the peak disappeared, which is consistent with the collapse of the gel above the VPT. The fit for the gel at 12.6 °C with eq 5 is shown in Figure 1a. Above T_{VPT}, when the gel is in the collapsed state, the gel model represented by eq 5 is no longer applicable.

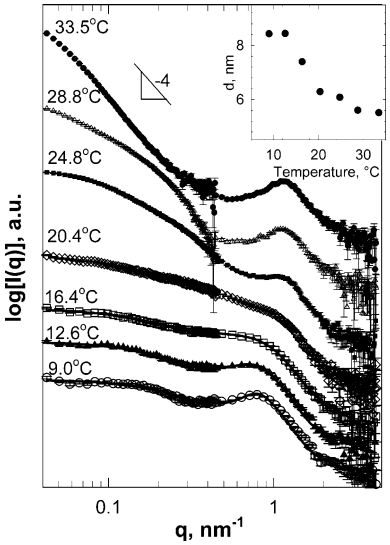

Figure 6. Temperature-dependent SANS for NF5 gels swollen with a mixture of $D_2O/H_2O = 10/90$. The curves obtained for different q ranges (see Experimental Section) were rescaled to improve clarity for comparisons. The water contents for samples at 9.0, 12.6, 16.4, 20.4, 24.8, 28.8, and 33.5 °C were 330, 287, 250, 185, 120, 110, and 105%, respectively.

Above $T_{VPT} = 17.8$ °C, the NIPA becomes hydrophobic, which results in dissociation of water and formation of polymer-poor (water-rich) domains within a collapsed, dense NIPA phase.[33] The SANS peak at $q_{max} = 0.9$ nm^{-1} due to the phase separation of the FOSA nanodomains disappeared, and a new peak due to phase separation of the water-rich nanodomains occurred at $q_{max} = 0.3$ nm^{-1} ($d = 21$ nm). A scattering peak for the FOSA nanodomains, which are expected to persist in this sample, is not resolved, which is a consequence of the larger scattering contrast between the NIPA and water-rich phases that masks the scattering from the FOSA nanodomains. As will be discussed below, when the ratio of D_2O/H_2O was varied to reduce the contrast between the NIPA and water phases, the scattering from the FOSA nanodomains is resolved. The aqueous nanodomains grew as the temperature increased, as can be seen from the shift of the SANS peak in Figure 5 to lower q. At 42.5 °C, Porod behavior, i.e., $I(q) \sim q^{-4}$, is clearly seen for $q < 0.5$ nm^{-1}, which indicates a sharp interface between the polymer and the water nanodomains.

The temperature dependence of the FOSA nanodomains was better seen for the SANS data using a D_2O/H_2O ratio of 10/90, which reduced the scattering contrast within the NIPA/water phase. A ratio of $D_2O/H_2O = 20/80$ would have been better for eliminating the scattering within the NIPA/water phase by matching their SLD's (see Table 3), but that ratio also reduced the contrast between the FOSA nanodomains and the NIPA/water phase (see Figure 3), which reduced the resolution of the FOSA nanodomain scattering. $D_2O/H_2O = 10/90$ represented a good compromise for studying the FOSA microstructure. The SANS curves for the NF5 gel are shown in Figure 6. The solid lines are the fit using the modified interacting core−shell model, eq 5, for gels at 9, 12.6, and 16.4 °C. The fitting parameters are summarized in Table 4. The fit for SANS at other higher temperatures was not successful since the model was not applicable above the VPT of the gel.

At temperatures below $T_{VPT} = 17.8$ °C, two peaks are visible: one at $q_{max} = 0.15$ nm^{-1} ($d = 41.9$ nm) and one at $q_{max} = 0.75$ nm^{-1} (8.4 nm). The higher q peak was due to the interdomain spacing of phase-separated FOSA nanodomains, and the lower q peak is believed to arise from a correlation length from clusters of FOSA nanodomains due to inhomogeneities in the spatial distribution of physical cross-links. The low-q intensity upturn that was observed in Figure 1a for this gel was absent in Figure 6 because of the lower contrast between the alkylacrylamide and the water. As a consequence, the large inhomogeneities represented by Ξ_2 was underestimated at 3.2−4.8 nm (see Table 4) compared with the value of 55.0 nm measured from Figure 1a.

As the temperature increased from 9 to 33.5 °C, the high-q peak shifted from $q_{max} = 0.75$ nm^{-1} ($d = 8.4$ nm) to $q_{max} = 1.2$ nm^{-1} ($d = 5.2$ nm) as a result of the interdomain spacing of the FOSA nanodomains becoming smaller due to collapse of the gel. The inset of Figure 6 shows that the interdomain spacing decreased substantially at the VPT. At 33.5 °C, the peak due to the microphase separation was observed at the same q as that for the dehydrated sample obtained from SAXS measurements.[1] That result indicates that the collapsed gel structure is similar to that of the dry copolymer even though it still contains 100 wt % water. The water is presumably totally contained within physically entrapped, aqueous domains in the collapsed gel as discussed above. The collapsed gels also were visibly cloudy, which indicates that, in addition to the inhomogeneities attributed to water nanodomains, larger size water clusters, large enough to scatter light, must also exist within the collapsed gel.

NF2, NF8, and NF10 exhibited similar temperature-dependent scattering patterns as the NF5 gel, except that the SANS for the NF2 gel showed no microphase separation peak, probably due to the relatively low FOSA compositions. As a consequence, the modified core−shell model, i.e., eq 5, did not fit the SANS for the NF2 gels. Neither did the model for the covalent gel, i.e., eq 1. This suggests that the hydrophobic interactions probably still produced a FOSA microphase but perhaps without the distinct shell structure that was seen in the other NF gels due to the lower FOSA composition. A model derived from eq 5 by simply replacing the form factor for the core−shell model with that for polydisperse hard spheres described by Griffith et al.[27] produced a satisfactory fit.

The model fitting parameters obtained for all the gels are summarized in Table 4. Since the model fit gives an effective hard-sphere radius, r_{eff}, and effective volume fraction of hard spheres, ϕ_{eff}, the average radius of the FOSA nanodomains r_0 can also be calculated from eq 7, which is based on the average volume fraction of FOSA nanodomains ϕ_0 obtained from swelling measurements[1]

$$r_0 = (\phi_0/\phi_{eff})^{1/3} r_{eff} \tag{7}$$

The aggregation number in the FOSA nanodomains was estimated by eq 8

$$N_{agg} = \frac{4\pi r_0^3 \rho N_A}{3M_{FOSA}} \tag{8}$$

where ρ, N_A, and M_{FOSA} are the density of the FOSA nanodomains, Avogadro's number, and the molecular weight of the FOSA monomer, respectively. The esti-

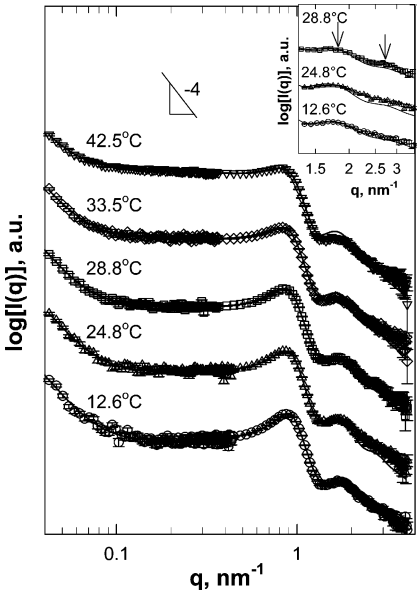

Figure 7. Temperature-dependent SANS for DF9 gels swollen with D_2O. The curves obtained for different q ranges (see Experimental Section) were rescaled to improve clarity for comparisons. The water contents for samples at 12.6, 24.8, 28.8, 33.5, and 42.5 °C were 180, 170, 165, 160, and 145%, respectively.

mated radius of the core r_0 and the aggregation number N_{agg} are listed in Table 4.

Figure 7 shows SANS curves for the DF9 gel in D_2O as a function of temperature. The solid lines show the fit of eq 5. The scattering curves did not change over the range of temperatures from 12.6 to 42.5 °C, which is in agreement with the absence of a VPT for the DF gels.[1] As discussed previously, the peak at $q_{max} = 1.7$ nm^{-1} is due to the core−shell form factor (cf. Figures 1 and 4), which from eq 6 corresponds to a radius of $r_a = 3.4$ nm for the core−shell nanodomains. Although the higher order peaks for the structure factor were not clearly resolved by the data in Figure 7, a second maximum in the form factor is visible at $q_{max} = 2.7$ nm^{-1} (see inset for Figure 7). For eq 6, the characteristic value for the second maximum for $q > 0$ is $k = 9.1$,[32] which for $q_{max} = 2.7$ nm^{-1} also produces a value of $r_a = 3.4$ nm. Higher order maxima for the form factor were not resolved.

Like the similar peak seen in Figure 4, the peak at $q_{max} = 0.85$ nm^{-1} ($d = 7.4$ nm) in the SANS data in Figure 7 is due to *inter*domain interference of the FOSA nanodomains. The upturn in the scattering intensity for $q < 0.1$ nm^{-1} is due to larger concentration fluctuations similar to those in the chemical DMA gel (see Figure 1 b). The other DF gels, DF5, DF17, and DF22, exhibited similar SANS scattering curves, and the structural parameters obtained from the model fits are listed in Table 4.

The model predictions for the radius of the core−shell nanodomains ($r_c + t$) of the DF gels were consistently ~3 nm; the core radius r_c ranged from 1.8 to 2.5 nm, and the shell thickness ranged from 0.6 to 1.2 nm. With increasing FOSA concentration, the core size, r_0, estimated from eq 7 increased from 1.8 to 3 nm, and the aggregation number, N_{agg}, estimated from eq 8 increased from 35 to 180. The polydispersity, p ($0 < p < 1$), was 0.1−0.15, which indicates that the core−shell nanodomains had a relatively narrow size distribution. The FOSA core radius r_c estimated from eq 7 increased from 1.8 to 2.4 nm for the DF22 gels when the temperature was increased from 12.6 to 42.5 °C, but it remained nearly constant for the DF9 gels. The changes in the DF22 gels may be due to coalescence of the FOSA nanodomains. Failure to see the same result for the DF9 gels may be a consequence of the much lower volume fraction of domains. Further studies of this are needed to resolve this difference in behavior.

For NF2 gels, the radius of the spherical FOSA nanodomains was 1.0 nm. For the other NF gels, the core radius, r_c, was ~ 2 nm, which was in good agreement with that calculated from eq 7, and the shell thickness, t, ranged from 0.8 to 1.5 nm. The aggregation number for the FOSA nanodomains, N_{agg}, ranged from 6 for the NF2 gels to between 30 and 60 for the other NF gels. The polydispersity varied from 0.2 to 0.25, which is higher than for DF gels and indicates that the core−shell nanodomains had a broader size distribution than did the DF gels.

Two sized inhomogeneities were observed for all the gels except the NF2 gels: a chain correlation length, ξ, that varied from 0.5 to 3.5 nm, which was due to the solutionlike thermal fluctuations of the chain in the water-rich phase, and a larger inhomogeneity, Ξ_2, due to a solidlike cluster structure in the gel that varied from 50 to 90 nm. As with the NF5 gels, the DF5, NF2, and NF8 gels swollen with a (10/90) D_2O/H_2O mixture did not exhibit a low-q upturn in the SANS due to the lower contrast between the alkylacrylamide and the water, and as a result, Ξ_2 calculated from the model fits of those data was underestimated. For the NF2 gels, the chain correlation length was not determined because of the strong incoherent scattering from the large amount of H_2O in the gel.

Conclusions

Hydrophobic interactions promoted nanophase separation of FOSA in both the DF and NF physical gels. The microstructure of these physical gels was significantly different from covalently cross-linked hydrogels in that the cross-link junctions of the physical gels consisted of FOSA nanodomains. The structure of the nanodomain junctions as determined from neutron scattering was consistent with a FOSA core surrounded by a water-depleted layer of the alkylacrylamide. The nanodomain junctions are distributed in a matrix of the water-swollen alkylacrylamide that exhibits chain size heterogeneities due to solutionlike thermal fluctuations. In addition, the hydrogels exhibited larger, solidlike inhomogeneities due to clustering of the polymer as a result of nonuniform swelling of the alkylacrylamide. Both the later heterogeneities are also commonly observed in covalently cross-linked gels.

The microstructures of the DF and NF gels exhibited different temperature dependencies. The NF gels shrank with increasing temperature, and the gels collapsed at the VPT, which is similar to the behavior of covalently cross-linked NIPA gels. The large inhomogeneities grew with temperature until macrophase separation of water from the polymer occurred above the VPT. The DF gel microstructure was relatively insensitive to changes in temperature between 10 and 45 °C.

Acknowledgment. We acknowledge the financial support from the Petroleum Research Fund of the American Chemical Society (Grant 36649-AC7) and Wesley Jessen Corp. We acknowledge the support of the

National Institute of Standards and Technology, U.S. Department of Commerce, in providing the neutron research facilities used in this work. The facilities at NIST are supported in part by the National Science Foundation under Agreement DMR-9986442. Discussions with Charles C. Han, Andrey Dobrynin, Charles J. Glinka, and Steven Kline are greatly appreciated. J.T. acknowledges the financial support for the SANS experiment from the University of Maryland Outreach Program. Certain commercial materials and equipment are identified in this paper in order to specify adequately the experiment procedure. In no case does such identification imply recommendation by the National Institute of Standards and Technology nor does it imply that the material or equipment identified is necessarily the best available for this purpose.

References and Notes

(1) Tian, J.; Seery, T. A. P.; Weiss, R. A. *Macromolecules* **2005**, *38*, 9994−10000.
(2) Dusek, K.; Patterson, D. *J. Polym. Sci., Polym. Phys. Ed.* **1968**, *6*, 1209−1216.
(3) Tanaka, T. *Phys. Rev. Lett.* **1978**, *40*, 820−823.
(4) de Gennes, P.-G. *Scaling Concepts in Polymer Physics*; Cornell University Press: Ithaca, NY, 1979.
(5) Higgins, J. S.; Benoit, H. C. *Polymers and Neutron Scattering*; Oxford University Press: New York, 1994.
(6) Stein, R. S. *J. Polym. Sci., Polym. Lett. Ed.* **1969**, *7*, 657−660.
(7) Wun, K. L.; Prins, W. *J. Polym. Sci., Polym. Phys. Ed.* **1974**, *12*, 533−543.
(8) Candau, S. J.; Young, C. Y.; Tanaka, T.; Lemarechal, P.; Bastide, J. *J. Chem. Phys.* **1979**, *70*, 4694−4700.
(9) Bastide, J.; Leibler, L. *Macromolecules* **1988**, *21*, 2647−2649.
(10) Tanaka, T.; Ishiwata, S. i.; Ishimoto, C. *Phys. Rev. Lett.* **1977**, *38*, 771−774.
(11) Shibayama, M.; Mizutani, S.-y.; Nomura, S. *Macromolecules* **1996**, *29*, 2019−2024.
(12) Wu, W.-l.; Shibayama, M.; Roy, S.; Kurokawa, H.; Coyne, L. D.; Nomura, S.; Stein, R. S. *Macromolecules* **1990**, *23*, 2245−2251.
(13) Shibayama, M.; Tanaka, T.; Han, C. C. *J. Chem. Phys.* **1992**, *97*, 6829−6841.
(14) Shibayama, M.; Tanaka, T.; Han, C. C. *J. Chem. Phys.* **1992**, *97*, 6842−6854.
(15) Shibayama, M.; Ikkai, F.; Satoshi, I.; Nomura, S.; Han, C. C. *J. Chem. Phys.* **1996**, *105*, 4358−4366.
(16) Mallam, S.; Horkay, F.; Hecht, A.-M.; Rennie, A. R.; Geissler, E. *Macromolecules* **1991**, *24*, 543−548.
(17) Horkay, F.; Hecht, A.-M.; Mallam, S.; Geissler, E.; Rennie, A. R. *Macromolecules* **1991**, *24*, 2896−2902.
(18) Li, Y.; Tanaka, T. *J. Chem. Phys.* **1989**, *90*, 5161−5166.
(19) Geissler, E.; Horkay, F.; Hecht, A.-M. *Phys. Rev. Lett.* **1993**, *71*, 645−648.
(20) Geissler, E.; Horkay, F.; Hecht, A.-M.; Rochas, C. *Polymer* **1997**, *38*, 15−20.
(21) Debye, P.; Bueche, A. M. *J. Appl. Phys.* **1949**, *20*, 518−525.
(22) Horkay, F.; McKenna, G. B.; Deschamps, P.; Geissler, E. *Macromolecules* **2000**, *33*, 5215−5220.
(23) Glinka, C. J.; Barker, J. G.; Hammouda, B.; Krueger, S.; Moyer, J. J.; Orts, W. J. *J. Appl. Crystallogr.* **1998**, *31*, 430−445.
(24) Hammouda, B.; Ho, D.; Kline, S. *Macromolecules* **2002**, *35*, 8578−8585.
(25) Pedersen, J. S.; Hamley, I. W.; Ryu, C. Y.; Lodge, T. P. *Macromolecules* **2000**, *33*, 542−550.
(26) Bartlett, P.; Ottewill, R. H. *J. Chem. Phys.* **1992**, *96*, 3306−3318.
(27) Griffith, W. L.; Triolo, R.; L.; C. A. *Phys. Rev. A* **1987**, *35*, 2200−2206.
(28) Percus, J. K.; Yevick, G. J. *Phys. Rev.* **1958**, *110*, 1−13.
(29) Horkay, F.; Hecht, A.-M.; Grillo, I.; Basser, P. J.; Geissler, E. *J. Chem. Phys.* **2002**, *117*, 9103−9106.
(30) Fournet, P. G. *Acta Crystallogr.* **1951**, *4*, 293.
(31) Kinning, D.; J.; Thomas, E. L. *Macromolecules* **1984**, *17*, 1712−1718.
(32) Guinier, A.; Fournet, G. *Small-Angle Scattering of X-rays*; John Wiley & Sons: New York, 1955; p 56.
(33) Shibayama, M.; Morimoto, M.; Nomura, S. *Macromolecules* **1994**, *27*, 5060−5066.

MA049474Z